Dephasing Dynamics across Different Local Vibrational Modes and Crystalline Environments

T. J. Keat,[1,2,3] D. J. L. Coxon,[1,2,4] M. Staniforth,[1,2] M. W. Dale,[5] V. G. Stavros,[2] M. E. Newton,[1,3,4] and J. Lloyd-Hughes[1,*]

[1]Department of Physics, University of Warwick, Coventry CV4 7AL, United Kingdom
[2]Department of Chemistry, University of Warwick, Coventry CV4 7AL, United Kingdom
[3]Warwick Centre for Doctoral Training in Diamond Science and Technology, University of Warwick, Coventry CV4 7AL, United Kingdom
[4]EPSRC Centre for Doctoral Training in Diamond Science and Technology, University of Warwick, Coventry CV4 7AL, United Kingdom
[5]De Beers Group, Belmont Road, Maidenhead SL6 6JW, United Kingdom

(Received 10 June 2022; revised 18 August 2022; accepted 20 October 2022; published 29 November 2022)

The perturbed free induction decay (PFID) observed in ultrafast infrared spectroscopy was used to unveil the rates at which different vibrational modes of the same atomic-scale defect can interact with their environment. The N_3VH^0 defect in diamond provided a model system, allowing a comparison of stretch and bend vibrational modes within different crystal lattice environments. The observed bend mode (first overtone) exhibited dephasing times $T_2 = 2.8(1)$ ps, while the fundamental stretch mode had surprisingly faster dynamics $T_2 < 1.7$ ps driven by its more direct perturbation of the crystal lattice, with increased phonon coupling. Further, at high defect concentrations the stretch mode's dephasing rate was enhanced. The ability to reliably measure T_2 via PFID provides vital insights into how vibrational systems interact with their local environment.

DOI: 10.1103/PhysRevLett.129.237401

Ultrafast infrared (IR) pump-probe spectroscopy is a powerful technique that is used across various fields of physics to track energy relaxation on femtosecond to nanosecond timescales [1]. This method has been applied in numerous studies of vibrational relaxation dynamics in liquid-phase molecular systems [2,3], thin-film polymers [4], and for crystallographic defects in semiconductors [5–8]. The vibrational dynamics of a system is described by the total dephasing rate $1/T_2$ [9,10] which includes population relaxation as well as the interactions between a vibrational system and its local environment [11,12]. The standard method of extracting T_2 via a Voigt profile fit to the IR absorption resonance often yields ambiguous results due to (i) the number of free parameters involved and (ii) the sensitivity of fitting routines to both initial parameters and data quality [13–16]. Therefore, it is desirable to explore alternative methods for the reliable extraction of T_2 from IR absorption features.

Perturbed free induction decay (PFID) offers a reliable method to directly measure T_2 in ultrafast pump-probe spectroscopy. It is observed in pump-probe measurements during negative time delays for systems with a T_2 longer than the probe pulse duration [17,18]. During negative time delays, the probe enters the system and induces a quantum coherent state, causing an optical signal known as free induction decay (FID) to be emitted. A subsequent pump pulse entering the system while the FID is being emitted will perturb the FID, producing a PFID signal that has a lifetime of T_2 [19,20]. PFID has been extensively reported in the literature for the vibrational transitions of various gas- and solution-phase compounds [20–22], and molecular systems at interfaces between materials [23,24]. Beyond vibrational transitions, PFID has also been observed in excitonic interactions [25,26] and electronic transitions [27]. While many studies ignore PFID or even try to actively filter it out [28], it can be used to measure T_2 associated with fundamental and overtone vibrational energy transitions [20]. However, the different local vibrational eigenmodes of a molecular defect embedded in a low-symmetry lattice may interact differently with their crystalline environment, which will be reflected in their T_2 lifetimes. Hence it is desirable to explore possible differences in the PFID response between stretch (S) and bend (B) vibrational modes, and the impact of differing local atomic environment. Such an investigation has been difficult to undertake as it requires controllably grown moleculelike systems that exhibit both types of vibrational transitions in a rigid lattice environment.

In this Letter we report the study, via PFID, of the T_2 lifetimes of the stretch and bend vibrational modes for crystallographic defects embedded in different local environments. The N_3VH^0 defect in diamond was used as a model system, with vibrational modes that yield IR absorption peaks at 2786 and 3107 cm^{-1}. These are

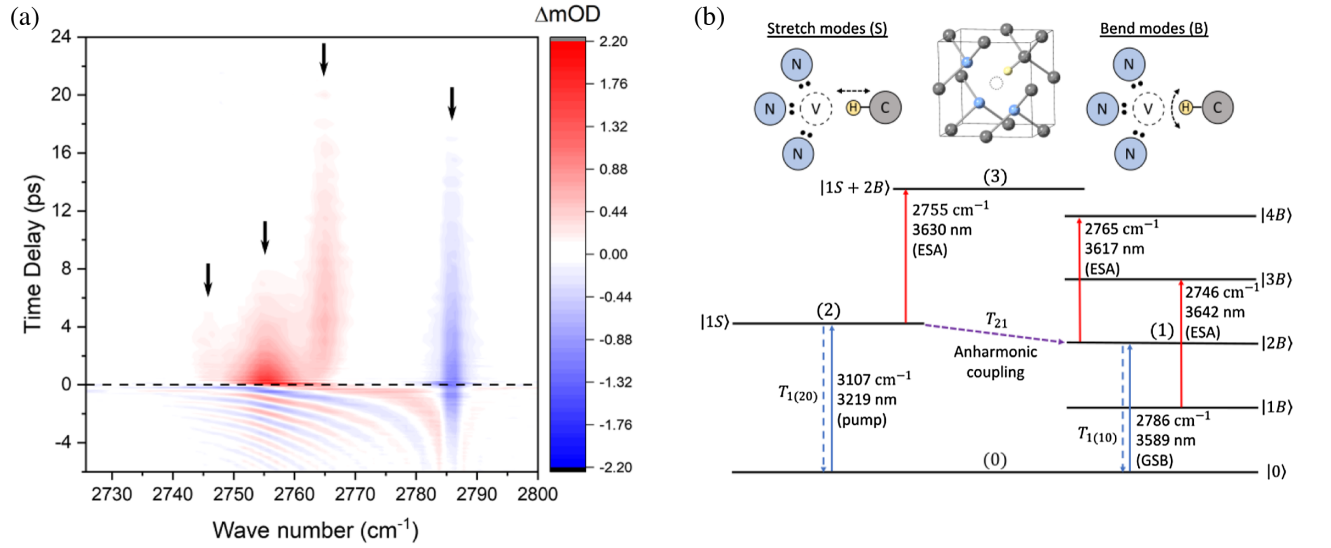

FIG. 1. (a) Transient optical density near the $2B$ mode for sample $N2$ under excitation with a 3107 cm^{-1} pump. Four features were observed in positive time delays, at 2746, 2755, 2765, and 2786 cm^{-1} as indicated by the black arrows. The dashed line marks zero time delay. PFID is evident at negative time delays. (b) Proposed energy level model for the N_3VH^0 defect, showing possible energy transition pathways. The $2B$ state gains population from $1S$ due to anharmonic coupling. Schematics of the N_3VH^0 defect show how the defect is embedded in a diamond lattice unit cell (middle) and also illustrate the C—H bond motion of the stretch (left) and bend (right) vibrational modes relative to the electron lone pairs (black dots) on the N atoms.

attributed respectively to the first bend mode overtone ($2B$) and the fundamental stretch mode ($1S$) of its C—H bond by experiments and first-principles theory [29–33]. Experiments were conducted on two natural diamonds ($N1$ and $N2$) and one synthetic diamond ($S1$) grown via chemical vapor deposition (CVD). Sample $N1$ was untreated, whereas $N2$ and $S1$ were annealed under high-pressure, high-temperature conditions to increase N_3VH^0 concentration [34–36]. Access to such controllably formed defects enables the exploration of how different local environments affects the PFID signal and T_2 of the same defect system. Our study reveals differences in the dephasing behavior of the S and B modes in the N_3VH^0 defect, of which the S mode dephasing appears more sensitive to the local environment.

We used ultrafast infrared pump-probe spectroscopy to conduct nondegenerate 3107 cm^{-1} pump, 2786 cm^{-1} probe experiments, as well as degenerate 3107 cm^{-1} pump-probe measurements [36]. Figure 1(a) illustrates pump-probe spectroscopy results obtained with a 3107 cm^{-1} pump, 2786 cm^{-1} probe. The ground state bleach (GSB) of the $2B$ mode was observed at 2786 cm^{-1}, along with an excited state absorption (ESA) feature at 2755 cm^{-1}, both of which started at zero pump-probe time delay. Given that the 2755 cm^{-1} ESA peaked at zero pump-probe delay and was close in wave number to the $2B$ mode, we assigned this resonance to the $1S$ to $1S + 2B$ transition. Two additional ESA features at 2746 and 2765 cm^{-1} both grew in after time zero, corresponding to transitions accessed after population transfer via anharmonic coupling to the B states, as summarized in Fig. 1(b). The positive time delay dynamics will be discussed elsewhere.

Here we focus primarily on the negative time delay dynamics, for which PFID was observed [Fig. 1(a)]. Prominent PFID oscillations branch away from the $2B$ resonance at 2786 cm^{-1}, with an oscillation period that decreased with larger detuning. The strength of the PFID signal was strongest near time zero at the 2786 cm^{-1} GSB and the 2755 cm^{-1} ESA. A "kink" in the PFID oscillations, evident from a change in signal intensity and curvature, was observed at 2755 cm^{-1}. The PFID signal of the 3107 cm^{-1} feature was also measured by conducting a degenerate 3107 cm^{-1} pump-probe measurement.

Previous works by Yan *et al.* [20] and Hamm and Zanni [37] provided a formalism to understand and model PFID by using perturbation theory in the interaction picture. Here we provide two crucial advances compared to previous models [20] by (i) incorporating a general treatment across different vibrational modes, and (ii) permitting different dephasing rates for each coherent quantum state induced by the pump and probe pulses, and enabling subtle changes in T_2 to be discerned. Our model is more widely applicable to materials with more complex energy structures, advancing PFID as a technique in the broader field of ultrafast spectroscopy. This is immensely useful as a method to measure T_2 as opposed to a Voigt function fitting, particularly for systems with spectrally overlapping features as exemplified in Fig. 1(a).

To facilitate discussion of our theoretical treatment, we labeled the relevant vibrational states according to their

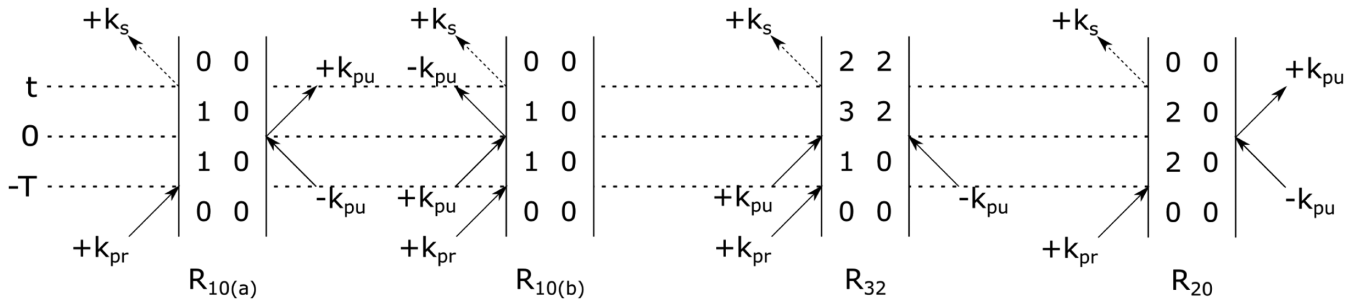

FIG. 2. Double-sided Feynman diagrams describing possible interactions in the nondegenerate 3107 cm^{-1} pump, 2786 cm^{-1} probe experiment ($R_{10(a)}$, $R_{10(b)}$, and R_{32}) and the degenerate 3107 cm^{-1} pump and probe experiment (R_{20}).

energy and number the ground, $2B$, $1S$, and $1S + 2B$ states as 0, 1, 2, and 3, respectively. The two ESA transitions with a delayed onset did not exhibit associated PFID signals. The PFID signal intensity [$S_{\mathrm{PFID}}(\omega)$] recorded by the infrared detector was linked to the electric fields of the probe pulse [$E_{\mathrm{pr}}(\omega)$] and of the PFID [$E_{\mathrm{sig}}(\omega)$], for which we assumed $E_{\mathrm{pr}}(\omega) \gg E_{\mathrm{sig}}(\omega)$. By further assuming that both the pump (158 fs) and probe (40 fs) pulses were much shorter than T_2 (valid since PFID was evident for longer than 6 ps), each pulse was approximated as a δ function in the semi-impulsive limit. In this approximation $E_{\mathrm{sig}}(\omega)$ is proportional to the response function of the defect, $R(\omega)$, giving the expression

$$S_{\mathrm{PFID}}(\omega) \propto \Re\{E^*_{\mathrm{pr}}(\omega)R(\omega)\}, \tag{1}$$

where $E^*_{\mathrm{pr}}(\omega) \propto e^{i\omega t}$.

The relevant double-sided Feynman diagrams (Fig. 2) of both the S and B modes of the N_3VH^0 system were considered, and demonstrate the interactions allowed for negative time delays. The response functions $R_{fi}(t_1, t_2, t_3)$ were constructed and labeled according to their corresponding positive time transition from initial state i to final state f:

$$R_{10}(T,0,t) \propto (|\mu_{10}|^2|\mu_{20}|^2 + |\mu_{10}|^2|\mu_{13}|^2) \times e^{-i\omega_{10}(t+T)}e^{-(t+T)/T_{2(10)}}, \tag{2}$$

$$R_{32}(T,0,t) \propto |\mu_{10}||\mu_{13}||\mu_{20}||\mu_{32}| \times e^{-i\omega_{10}T}e^{-T/T_{2(10)}}e^{-i\omega_{32}t}e^{-t/T_{2(32)}}, \tag{3}$$

$$R_{20}(T,0,t) \propto |\mu_{20}|^4 e^{-i\omega_{20}(t+T)}e^{-(t+T)/T_{2(20)}}, \tag{4}$$

where t_1 is the time at which the probe interacts with the system, t_2 is the time at which the pump interacts, t_3 is the time at which the signal field is emitted, and T is the pump-probe delay magnitude. μ_{fi} are the transition dipole moments, and subscripts f and i denote the corresponding vibrational states. Feynman diagrams describing negative time delay interactions at 2746 and 2765 cm^{-1} could not be constructed, which suggests that these positive time features do not have a corresponding PFID signal.

The PFID response was obtained by taking the Fourier transform of Eqs. (2)–(4) and substituting into Eq. (1). The total PFID response $S(T,\omega)$ of the system was then obtained by the summation of all the possible PFID signals occurring within the probe pulse bandwidth. When the $2B$ region was probed, as in Fig. 1(a), the total PFID response was given by

$$S_{2786}(T,\omega) \propto e^{-T/T_{2(10)}} \times \frac{(1/T_{2(10)})\cos[(\omega-\omega_{10})T] - (\omega-\omega_{10})\sin[(\omega-\omega_{10})T]}{(\omega-\omega_{10})^2 + (1/T_{2(10)})^2} - re^{-T/T_{2(10)}} \times \frac{(1/T_{2(32)})\cos[(\omega-\omega_{10})T] - (\omega-\omega_{32})\sin[(\omega-\omega_{10})T]}{(\omega-\omega_{32})^2 + (1/T_{2(32)})^2}, \tag{5}$$

which includes PFID contributions from R_{10} and R_{32}, with r as the ratio between the two. At $\omega = \omega_{10}$, Eq. (5) gives $T_{2(10)}$ via an exponential fit. Simulating the PFID around 2755 cm^{-1} and comparing it to experimental data further allows an estimate of $T_{2(32)}$. The PFID response at 3107 cm^{-1} is described by

$$S_{3107}(T,\omega) \propto e^{-T/T_{2(20)}} \times \frac{(1/T_{2(20)})\cos[(\omega-\omega_{20})T] - (\omega-\omega_{20})\sin[(\omega-\omega_{20})T]}{(\omega-\omega_{20})^2 + (1/T_{2(20)})^2}, \tag{6}$$

where only R_{20} contributes to the PFID and $T_{2(20)}$ is obtained with an exponential fit at $\omega = \omega_{20}$.

We extracted T_2 based on Eqs. (5) and (6) for all samples, as summarized in Table I. The value of $T_{2(10)}$ agreed across all samples, with an average of 2.8 ± 0.1 ps. The agreement between the three samples demonstrates reliability in using PFID to measure dephasing times. However, a discrepancy between sample $N1$ and samples

TABLE I. Dephasing times obtained from PFID fitting (ps).

	$N1$	$N2$	$S1$
$T_{2(10)}$	2.87 ± 0.07	2.8 ± 0.1	2.8 ± 0.2
$T_{2(20)}$	1.14 ± 0.02	1.69 ± 0.07	1.64 ± 0.07

$N2$ and $S1$ was observed for $T_{2(20)}$. Sample $N1$ gave $T_{2(20)} = 1.14 \pm 0.02$ ps, lower than the average value of 1.67 ± 0.05 ps for $N2$ and $S1$, indicating a distinct dephasing behaviour for the $1S$ mode, discussed later.

The value of $T_{2(10)}$ (C—H bend) was longer than $T_{2(20)}$ (C—H stretch) for all samples. The dephasing time is determined by the coupling between a defect and its local environment, particularly to the crystal lattice phonons [11,12]. Hence, our results suggest a stronger coupling between the C—H stretch and the local lattice environment compared to the C—H bend. To explain this phenomenon, one can consider a simple spring model of the C—H bond within the N_3VH^0 structure. Stretching the C—H bond moves the H atom towards the three N atoms in the defect and their lone pairs [Fig. 1(b)], perpendicular to the potential energy contour of the defect. This causes the H atom to observe a larger change in potential compared to bending the C—H bond, where the H atom oscillates at a similar radial distance from the lone pairs and along the potential energy contour. The S mode vibration therefore produces a larger change in potential for the H atom, creating a larger perturbation to the local crystal lattice in comparison to the B mode. This enhances phonon scattering processes for the S mode, leading to stronger coupling with the crystal lattice and higher dephasing rate $1/T_2$ relative to the B mode. A similar behavior has been observed in molecular water, in which S mode vibrations exhibit stronger intermolecular coupling compared to B mode vibrations [38].

The PFID response was simulated for the S and $2B$ regions using Eqs. (5) and (6). The ratio between the magnitudes of the experimental signal at 2786 and 2755 cm^{-1} near time zero gave $r = 1.05$, 0.98, and 1.13 for $N1$, $N2$, and $S1$, respectively. Figure 3 compares the simulated and experimental results from sample $N2$. Figures 3(a) and 3(b) indicate that the essential features of the PFID around the $2B$ region, such as the prominent oscillations at lower wave numbers, are well reproduced by theory. Notably, the PFID is broad enough in wave number that it extends from the 2786 cm^{-1} feature to the ESA features at 2755 cm^{-1}. The change in PFID oscillation intensity and curvature below 2755 cm^{-1} is controlled by the parameter $T_{2(32)}$, with a larger value yielding a more abrupt change in signal [36]. The best qualitative fit was obtained with $T_{2(32)} \approx 1.0 \pm 0.2$ ps for all samples. Reasonable fits could not be obtained with $T_{2(32)} = T_{2(10)}$ [36], as assumed in previous work [20]. When multiple coherent states are involved, their dephasing rates must be considered individually. The shorter $T_{2(32)}$ compared to $T_{2(10)}$ and $T_{2(20)}$ could result from the higher population relaxation rates for excited states. More importantly, our results demonstrate that PFID can distinguish between dephasing times of different coherent states. This cannot be achieved via equilibrium methods such as Fourier transform infrared spectroscopy (FTIR), and is challenging to do in standard pump-probe spectroscopy when multiple resonances overlap spectrally [e.g., in the 2740–2770 cm^{-1} in Fig. 1(a)]. This opens open a new research avenue in ultrafast spectroscopy, in which the dephasing rates for coherent states between nonequilibrium energy levels can now be precisely determined.

Figures 3(c) and 3(d) show that the PFID around 3107 cm^{-1} was also well described, with a form similar to the PFID around 2786 cm^{-1}. Figure 3(e) compares the experimental and simulated PFID for all samples at 2786 cm^{-1}. The two demonstrate good agreement, highlighting the validity in using Eqs. (5) and (6) to simulate PFID and extract T_2. Subtle differences can be observed between model and experiment: for example, the experimental PFID signals for 3107 and 2786 cm^{-1} were both asymmetric, with reduced intensity at higher wave numbers, which was not fully captured in the simulation.

We now return to a discussion of the different values of $T_{2(20)}$ seen for the $1S$ state. The varying $T_{2(20)}$ suggests that

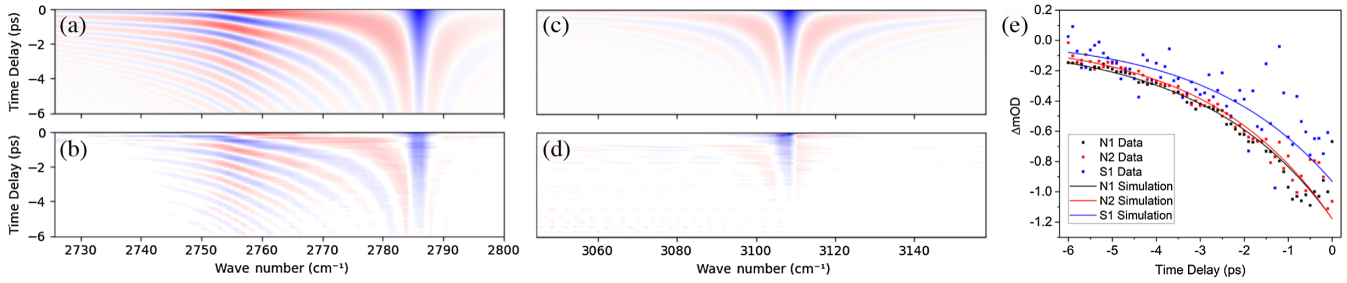

FIG. 3. (a) Simulated and (b) experimental PFID signal for the 3107 cm^{-1} pump, 2786 cm^{-1} probe measurement on sample $N2$. (c) Simulated and (d) experimental PFID signal for the degenerate 3107 cm^{-1} pump-probe measurement on $N2$. (e) Comparison between simulated data and experimental data at the 2786 cm^{-1} feature for all samples.

TABLE II. Concentration of common nitrogen-related defects found in samples $N1$, $N2$, and $S1$ in parts per million (ppm).

Sample	N_s^0	A centers	B centers	N_3VH^0
$N1$	< 1	< 1	940 ± 90	44 ± 4
$N2$	< 1	115 ± 7	200 ± 20	13 ± 1
$S1$[a]	8 ± 3[b]	< 17[c]	< 9[c]	4.2 ± 0.4

[a]The FTIR spectrum of $S1$ could not be resolved for N_s^0 and A/B centers.
[b]Obtained via electron paramagnetic resonance (EPR) measurements instead of FTIR.
[c]The upper limits for A/B center concentrations based on the concentrations of N_s^0, N_3VH^0, and the known total nitrogen concentration in $S1$.

the S mode vibrations are sensitive to local crystal lattice conditions. We consider variations in diamond defect concentrations as a factor contributing to differences in the local crystal environment. FTIR spectroscopy was conducted to extract the concentration of common nitrogen-related diamond defects in our samples, including substitutional nitrogen (N_s^0), A centers, B centers, and N_3VH^0. The N_3VH^0 concentration was obtained from the area of the 3107 cm^{-1} absorption feature via the calibration factor of 110 ± 10 ppb/cm^2 [35]. The concentration of other defects were obtained via fitting a known reference spectrum of each defect [39]. The results of these measurements are summarized in Table II. The total concentration of nitrogen-related defects, in particular the B centers, is much higher in sample $N1$ compared to the other samples. Viewing $N1$ through crossed polarizers also shows significant dislocations throughout the sample. The shorter $T_{2(20)}$ in $N1$ could originate from either the higher concentrations of point defects (B centers) and dislocations either enhancing lattice phonon scattering via crystal lattice perturbations, or introducing additional states that act as extra dephasing pathways.

In summary, we have demonstrated PFID as a method to investigate T_2 for both the S and B vibrational modes of atomic-scale defects, using the N_3VH^0 diamond defect as a model system. The demonstrated difference in T_2 for different vibrational eigenmodes and lattice conditions reveals an intrinsic connection between the dephasing dynamics, potential energy contour, and local environment of a molecular system. Rather than ignoring or filtering away PFID as a "coherent artifact" of pump-probe measurements [28], PFID may serve as a powerful tool in optics and ultrafast spectroscopy by providing subtle features that, when modeled accurately, yield accurate dephasing rates. These advances will be of interest in (i) chemical physics, where PFID as a spectroscopic technique is widely applicable to study the ultrafast vibrational dynamics of solid-state, liquid-phase, and gas-phase molecular systems [20–27]; (ii) molecular chemistry, where using PFID to accurately measure T_2 across different vibrational modes would advance the molecular design of popular systems such as modified graphene [40] and dye molecules [41], and could also uncover key molecule-environment interactions [42]; and (iii) semiconductor and quantum physics, where PFID may be used to probe defect-lattice interactions within tailored defect environments in diamond, as in the present work, or indeed in other semiconductor materials with important functional defects, such as GaN [43], silicon [44], or metal oxides [45].

T. J. K. would like to acknowledge financial support from the De Beers Group and Warwick Centre for Doctoral Training in Diamond Science and Technology. V. G. S. would like to thank the Royal Society for a Royal Society Industry Fellowship. We thank H. S. Tan (Nanyang Technological University) for insightful discussions regarding PFID. We thank B. G. Breeze (University of Warwick) for providing EPR data on sample $S1$. We thank J. Chapman (Gemetrix Pty Ltd) for the provision of sample $N1$. We thank the De Beers Group for the provision of sample $N2$. We thank D. A. Braje (MIT Lincoln Laboratory) for provision of sample $S1$.

*J.Lloyd-Hughes@warwick.ac.uk

[1] J. Lloyd-Hughes *et al.*, J. Phys. Condens. Matter **33**, 353001 (2021).
[2] S. Woutersen and H. J. Bakker, Phys. Rev. Lett. **96**, 138305 (2006).
[3] D. J. Shaw, M. R. Panman, and S. Woutersen, Phys. Rev. Lett. **103**, 227401 (2009).
[4] O. Selig, R. Siffels, and Y. L. A. Rezus, Phys. Rev. Lett. **114**, 233004 (2015).
[5] M. Budde, G. Lüpke, C. P. Cheney, N. H. Tolk, and L. C. Feldman, Phys. Rev. Lett. **85**, 1452 (2000).
[6] M. Budde, G. Lüpke, E. Chen, X. Zhang, N. H. Tolk, L. C. Feldman, E. Tarhan, A. K. Ramdas, and M. Stavola, Phys. Rev. Lett. **87**, 145501 (2001).
[7] G. Lüpke, N. H. Tolk, and L. C. Feldman, J. Appl. Phys. **93**, 2317 (2003).
[8] R. Ulbricht, S. T. van der Post, J. P. Goss, P. R. Briddon, R. Jones, R. U. A. Khan, and M. Bonn, Phys. Rev. B **84**, 165202 (2011).
[9] E. Rosencher and B. Vinter, *Optoelectronics*, edited by P. G. Piva (Cambridge University Press, Cambridge, England, 2002).
[10] M. Chachisvilis, H. Fidder, and V. Sundström, Chem. Phys. Lett. **234**, 141 (1995).
[11] T. Kiviniemi, J. Aumanen, P. Myllyperkiö, and M. Pettersson, in *Femtochemistry VII*, edited by A. W. Castleman and M. L. Kimble (Elsevier, Amsterdam, 2006), pp. 39–43.
[12] F. Laussy, E. Del Valle, T. München, A. Laucht, A. Gonzalez-Tudela, M. Kaniber, J. Finley, and C. Tejedor, in *Quantum Optics with Semiconductor Nanostructures*, edited by F. Jahnke (Woodhead Publishing, Cambridge, England, 2012), pp. 293–331.

[13] G. Lei, J. E. Anderson, M. I. Buchwald, B. C. Edwards, and R. I. Epstein, Phys. Rev. B **57**, 7673 (1998).
[14] E. Neu, C. Hepp, M. Hauschild, S. Gsell, M. Fischer, H. Sternschulte, D. Steinmüller-Nethl, M. Schreck, and C. Becher, New J. Phys. **15**, 043005 (2013).
[15] S. Koirala, S. Mouri, Y. Miyauchi, and K. Matsuda, Phys. Rev. B **93**, 075411 (2016).
[16] N. Stavrias, K. Saeedi, B. Redlich, P. T. Greenland, H. Riemann, N. V. Abrosimov, M. L. W. Thewalt, C. R. Pidgeon, and B. N. Murdin, Phys. Rev. B **96**, 155204 (2017).
[17] K. Wynne and R. Hochstrasser, Chem. Phys. **193**, 211 (1995).
[18] F. Rossi and T. Kuhn, Rev. Mod. Phys. **74**, 895 (2002).
[19] P. Hamm, Chem. Phys. **200**, 415 (1995).
[20] S. Yan, M. T. Seidel, and H.-S. Tan, Chem. Phys. Lett. **517**, 36 (2011).
[21] N. C. Cole-Filipiak, J. Troß, P. Schrader, L. M. McCaslin, and K. Ramasesha, J. Chem. Phys. **154**, 134308 (2021).
[22] M. Banno, A. Kotani, K. Ohta, and K. Tominaga, Bull. Chem. Soc. Jpn. **87**, 470 (2014).
[23] K.-i. Inoue, M. Ahmed, S. Nihonyanagi, and T. Tahara, Nat. Commun. **11**, 5344 (2020).
[24] J. Tan, B. Zhang, Y. Luo, and S. Ye, Angew. Chem., Int. Ed. Engl. **56**, 12977 (2017).
[25] T. Guenther, C. Lienau, T. Elsaesser, M. Glanemann, V. M. Axt, T. Kuhn, S. Eshlaghi, and A. D. Wieck, Phys. Rev. Lett. **89**, 057401 (2002).
[26] Y. Murotani, M. Takayama, F. Sekiguchi, C. Kim, H. Akiyama, and R. Shimano, J. Phys. D **51**, 114001 (2018).
[27] J. M. Richter, F. Branchi, F. V. de Almeida Camargo, B. Zhao, R. H. Friend, G. Cerullo, and F. Deschler, Nat. Commun. **8**, 376 (2017).
[28] T. Polack, Opt. Express **14**, 5823 (2006).
[29] E. Fritsch, T. Hainschwang, L. Massi, and B. Rondeau, New Diamond Front. Carbon Technol. **17**, 63 (2007).
[30] G. Davies, A. T. Collins, and P. Spear, Solid State Commun. **49**, 433 (1984).
[31] I. Kiflawi, D. Fisher, H. Kanda, and G. Sittas, Diam. Relat. Mater. **5**, 1516 (1996).
[32] J. P. Goss, P. R. Briddon, V. Hill, R. Jones, and M. J. Rayson, J. Phys. Condens. Matter **26**, 145801 (2014).
[33] F. S. Gentile, S. Salustro, M. Causà, A. Erba, P. Carbonniére, and R. Dovesi, Phys. Chem. Chem. Phys. **19**, 22221 (2017).
[34] M. N. R. Ashfold, J. P. Goss, B. L. Green, P. W. May, M. E. Newton, and C. V. Peaker, Chem. Rev. **120**, 5745 (2020).
[35] D. J. L. Coxon, M. Staniforth, B. G. Breeze, S. E. Greenough, J. P. Goss, M. Monti, J. Lloyd-Hughes, V. G. Stavros, and M. E. Newton, J. Phys. Chem. Lett. **11**, 6677 (2020).
[36] See Supplemental Material at http://link.aps.org/supplemental/10.1103/PhysRevLett.129.237401 for further details about experimental and theoretical methods.
[37] P. Hamm and M. Zanni, *Concepts and Methods of 2D Infrared Spectroscopy* (Cambridge University Press, Cambridge, England, 2011).
[38] C.-C. Yu, K.-Y. Chiang, M. Okuno, T. Seki, T. Ohto, X. Yu, V. Korepanov, H.-o. Hamaguchi, M. Bonn, J. Hunger, and Y. Nagata, Nat. Commun. **11**, 5977 (2020).
[39] M. W. Dale, Colour centres on demand in diamond, Ph.D. thesis, University of Warwick, 2015.
[40] H. S. AlSalem and S. P. K. Koehler, J. Phys. Chem. C **126**, 7571 (2022).
[41] Y. Yoneda, B. Kudisch, S. Rafiq, M. Maiuri, Y. Nagasawa, G. D. Scholes, and H. Miyasaka, J. Am. Chem. Soc. **143**, 14511 (2021).
[42] B. Grüner, M. Schlesinger, P. Heister, W. T. Strunz, F. Stienkemeier, and M. Mudrich, Phys. Chem. Chem. Phys. **13**, 6816 (2011).
[43] S. Suihkonen, S. Pimputkar, S. Sintonen, and F. Tuomisto, Adv. Electron. Mater. **3**, 1600496 (2017).
[44] L. I. Murin, S. B. Lastovskii, E. A. Tolkacheva, V. P. Markevich, A. R. Peaker, and B. G. Svensson, Phys. Status Solidi (a)**213**, 2850 (2016).
[45] W. M. Hlaing Oo, S. Tabatabaei, M. D. McCluskey, J. B. Varley, A. Janotti, and C. G. Van de Walle, Phys. Rev. B **82**, 193201 (2010).